J. Mech. Phys. Solids 154 (2021) 104511

Contents lists available at ScienceDirect

Journal of the Mechanics and Physics of Solids

journal homepage: www.elsevier.com/locate/jmps

On the role of pre-existing defects in influencing hardness in nanoscale indentations — Insights from atomistic simulations

Ashish Chauniyal [a,*], Gerhard Dehm [b], Rebecca Janisch [a]

[a] Interdisciplinary Centre for Advanced Materials Simulation (ICAMS) Ruhr-Universität Bochum, 44780 Bochum, Germany
[b] Max-Planck-Institut für Eisenforschung GmbH, Max-Planck-Str.1, Düsseldorf 40237, Germany

ARTICLE INFO

Keywords:
Indentation and hardness (A)
Strengthening and mechanisms (A)
Pre-existing defects (B)
Numerical algorithms (C)

ABSTRACT

Using in-situ nanoindentation experiments it is possible to study the dislocation mechanisms which unfold under an indenter.Large-scale atomistic simulations of the same are possible due to similarities in length scale, provided that defects can be included in the simulation. Yet, nanoindentation simulations have so far been mostly undertaken on defect free samples, while studies with pre-existing defects are few. The latter show that the average hardness is not affected by the presence of pre-existing defects, which justifies the use of ideal crystals in such simulations. However, this observation is counter-intuitive, as indenter-defect interactions should lead to work hardening and manifest themselves in hardness calculations. Our simulations along with a new look at the evolution of dislocations under the indenter, show for the first time, that hardness in atomistic simulations is influenced by pre-existing defects in the sample. Utilizing a face-centred tetragonal TiAl bicrystal with misfit dislocations at the interface, to populate the sample with defects, we correlate the contact-pressure variations to defect-indenter interactions. We show that the measured contact-pressure is affected by the presence and nature of defects under the indenter. Dislocation pile ups lead to intermittent rise in contact pressure, while seamless growth leads to steady convergence. The sensitivity to detect such defect interactions depends upon indenter size while convergence to average hardness is a result of curvature accommodation near the surface. Our findings prove that pre-existing defects have a profound influence on calculated hardness in indentation simulations which also corroborates with experimental observations in the literature.

1. Introduction

Large scale atomistic simulations of deformation, which otherwise were conducted using dislocation free crystals, have recently shown promising developments by including pre-existing defects (Zepeda-Ruiz et al., 2017; Ko et al., 2020). Thus, realistic defect interactions can now be studied while distinctly resolving defect evolution. Consequently, the results have also been successfully correlated to experimental studies (Ko et al., 2020).

Hitherto, atomistic simulations of *nanoindentation* were also undertaken using ideal dislocation free crystals (Begau et al., 2011; Kelchner et al., 1998; Ziegenhain et al., 2015; Voyiadjis and Yaghoobi, 2017; Zimmerman et al., 2009) while simulations with pre-existing defects in the crystal sample were performed sparingly (Alabd Alhafez et al., 2019; Ukwatta and Achuthan, 2014; Lodes et al., 2011; Njeim and Bahr, 2010; Salehinia and Bahr, 2012). Recent studies with pre-existing defects in BCC crystals suggests that

* Corresponding author.
E-mail address: ashish.chauniyal@rub.de (A. Chauniyal).

https://doi.org/10.1016/j.jmps.2021.104511
Received 22 February 2021; Received in revised form 28 April 2021; Accepted 25 May 2021
Available online 1 June 2021

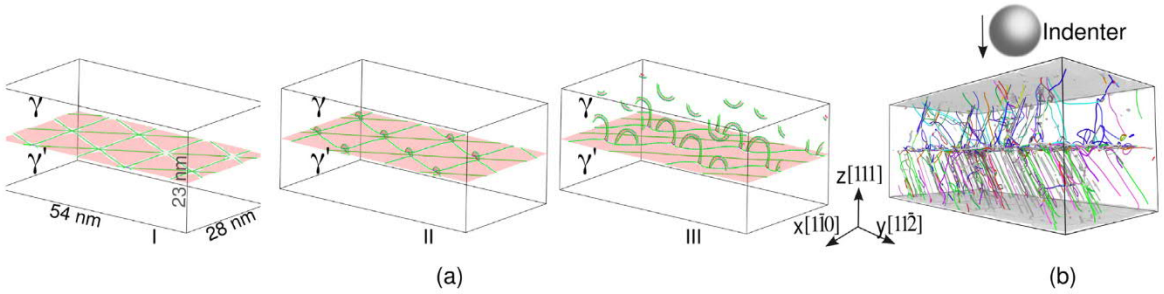

Fig. 1. Method to populate sample bi-crystal with dislocations. (a) The structure of the γ-pseudo twin misfit interface (b) Simulation volume filled with dislocations before the start of indentation, using a spherical indenter.

the average hardness is not influenced by pre-existing dislocations, thereby, justifying the use of ideal crystals for nanoindentation simulations (Alabd Alhafez et al., 2019).

This conclusion is counter-intuitive, as one expects some signature of work hardening due to indenter-defect interactions (Shankar et al., 2005; Montagne et al., 2013; Oliver and Pharr, 1992; Fischer-Cripps and Nicholson, 2004; Phani et al., 2013; Catoor et al., 2013; Bei et al., 2016; Shim et al., 2008; Morris et al., 2011; Xia et al., 2016; Pharr et al., 2010; Choi et al., 2013; Derlet and Maaß, 2016; Barnoush, 2012) in the sample, which could not be observed. For instance multiple in-situ indentation studies (Minor et al., 2006; Morris et al., 2007; Lee et al., 2020; Ohmura et al., 2004; Liu et al., 2014; Bufford et al., 2014) show how defects nucleated under the indenter can interact with the underlying microstructural features. In fact, Bufford et al. (2014) have clearly observed pre-existing threading dislocations to detach from the surface into the specimen, and repeated indentation on the same position leads to higher indentation stress. The same relation between dislocation density and flow stress has already been studied using atomistic simulations (Zepeda-Ruiz et al., 2017), which shows that hardening due to interacting dislocations can be captured using atomistic simulations as well. Thus it is surprising that particularly during nanoindentation simulations, such effects are not manifested in contact-pressure measurements itself.

It is therefore imperative, that the influence of pre-existing defects on indentation response is studied using atomistic simulations which are able to resolves various atomic mechanisms during defect evolution and correlate them with known phenomena in experimental observations.

There is a key caveat to consider when undertaking such a study. Due to the small indenter size (a few nanometres) only a small fraction of the sample is indented upon. Since the indenter creates a very localized stress field a large part of the sample does not interact with the indenter (Morris et al., 2007; Minor et al., 2006; Shim et al., 2008; Morris et al., 2011; Jin et al., 2018), while the defects directly under the indenter can have a strong influence on the indentation response (Alabd Alhafez et al., 2019; Ukwatta and Achuthan, 2014; Shankar et al., 2005; Barnoush, 2012; Bei et al., 2016, 2008; Patel and Lee, 2020). Thus, in small scale indentations the dislocation density of the sample (Taylor, 1938; Liu et al., 2019) conveys little information regarding the complex stress states near the indenter. Instead, the position of the indentation should be the overriding factor, as the sample defects are in-homogeneously distributed (Montagne et al., 2013; Morris et al., 2011; Shim et al., 2008), making it imperative to perform indentation at different positions. Moreover, such a study will most directly mimic the experimental specimens with pre-existing dislocations used in numerous studies (Ohmura et al., 2004; Bufford et al., 2014; Morris et al., 2007; Barnoush, 2012; Morris et al., 2011; Shim et al., 2008).

In this paper we simulate nanoindentation over a sample with pre-existing defects and study its indentation response. We use a realistic defect population method, where misfit dislocations at semi-coherent γ/γ' TiAl interface are used to nucleate a dislocation forest. By indenting at different positions of the sample, we show that defect interactions can alter the measured hardness which is also sensitive to the position of indentation. The sensitivity to detect these interactions can, however, change depending upon the indenter size where a large indenter is most suitable as it responds to a large number of sample defects. Our findings are essential, firstly, for the simulation community, as they usher a gradual shift towards simulating large scale realistic microstructures, and secondly, for the in-situ experimental community, which can better estimate the nature of defect evolution under the indenter and correlate it with measured stresses.

2. Methods

2.1. Simulation details

Molecular dynamics simulations are performed using an embedded atom method (EAM) potential by Zope and Mishin (2003) with LAMMPS simulations package (Plimpton, 1995). The potential is shown to correctly predict the properties of intermetallic TiAl along with specific dislocation interactions (Chauniyal and Janisch, 2020). To visualize the snapshots of our simulations we use OVITO package (Stukowski and Albe, 2010) and an inbuilt dislocation extraction algorithm (Stukowski et al., 2012).

The simulation box, shown in Fig. 1, measures 28 nm×54 nm×23 nm along x y and z directions respectively and contains ~ 2 200 000 atoms. The thickness along z direction is sufficient to avoid any thin film effects (Nair et al., 2008). To obtain a defective crystal,

uniaxial tensile tests are carried out at 1 K temperature, maintained using a Nose–Hoover thermostat (NVT) and full periodic boundary conditions. This is followed by unloading and relaxation with free surface conditions along $z[111]$ to prepare for indentation.

Nanoindentation simulations are performed at 1 K to minimize thermal effects on dislocation movement and interactions using Nose–Hoover thermostat at constant volume (NVT). We perform indentations over a *defective bi-crystal* shown in Fig. 1(b), along with a *defect free crystal*, which is a pristine γ crystal without a twin boundary. A few atomic layers at the bottom of the sample are fixed to prevent any translational movement during indentation.

The indenter is modelled as a repulsive sphere having a radius of $R = 80$ Å where the interaction potential with other atoms is described as:

$$V(r) = \begin{cases} k(R-r)^2, & r < R, \\ 0, & r \geq R. \end{cases} \tag{1}$$

where r is the distance of any atoms to the indenter centre and the indenter stiffness is kept constant at $k = 10$ eV/Å^2. It is typical to use an atomically flat, infinitely rigid indenter, as long as the focus remains on the physics of the sample. The indenter is driven towards the sample at a constant velocity of 0.1 Å/ps from a starting position above the surface. When the indenter comes in contact with the sample a normal force F_z is directly recorded on indenter. Following which a contact stress can be calculated by dividing the force (F_z) by a suitable contact area.

During indentation the contact area changes rapidly, which makes the *choice of contact area* crucial in determining contact pressure. Moreover, due to atomic resolution the contact area is difficult to determine, as not all atoms underneath the indenter are always in direct contact (Ziegenhain et al., 2015). A simple method is to directly estimate the contact area by using an analytic expression as a function of instantaneous depth h (Alabd Alhafez et al., 2019). This method, however, leads to an overestimation of contact area. Instead, we use a more accurate method by calculating the positions of atoms in contact at the periphery of the indenter (Ziegenhain et al., 2015). This gives us an elliptic contact area which is calculated as:

$$A^{elliptic} = \frac{\pi}{4}(x^{max} - x^{min})(y^{max} - y^{min}) \tag{2}$$

where x and y measure the coordinates of the contact atoms projected into the surface plane which is described as a curved contour line which approximates as an ellipse. The above method is directly implemented in LAMMPS (Ziegenhain et al., 2015) to output the corresponding force and contact area.

2.2. Inducing defects in the crystal

To prepare the specimen for indentation, defects need to be introduced in the specimen. Defects are generally artificially induced in crystals using various methods, such as vacancy annealing and half plane removal (Zepeda-Ruiz et al., 2017; Alabd Alhafez et al., 2019; Ukwatta and Achuthan, 2014). However, in this study we nucleate dislocations from misfit dislocations at γ/γ' twin interface, which is more realistic and produces glissile dislocation segments. The role of misfit interfaces as alternate nucleation sources is well known (Salehinia et al., 2014; Zhang et al., 2012) and using this technique we simulate the same mechanism.

The use of γ-TiAl system is essential, as its face centred tetragonal (FCT) crystal structure allows for rotational twin variants — pseudo twin PT, rotational boundary RB, true twin TT. While a $\gamma - TT$ interface is inherently coherent, a $\gamma - PT$ twin interface exhibits misfit dislocations (Appel et al., 2011). We construct a $\gamma - PT$ bilayer structure by rotating one γ layer over the other by 60°, while ensuring periodic boundary conditions. The structure is then minimized and relaxed to obtain a $\gamma - PT$ twinned bi-layer having misfit dislocations as shown in Fig. 1(a.I).

To populate the bi-crystal with dislocations, a uniaxial tensile strain is applied along the $x[1\bar{1}0]$ direction, during which the periodically repeating misfit dislocations nucleate new dislocations into the crystal. The initial stages of nucleation and propagation are shown in Fig. 1(a.II,a.III). After straining the system up to 0.05 strain, the structure is unloaded and relaxed. This is followed by another relaxation with free surface boundary condition along $z = [111]$ direction, to prepare the sample for indentation simulations. The thus prepared *defective crystal* sample, with a dense dislocation forest is shown in Fig. 1(b) on which indentation is performed using a spherical indenter.

The advantage of using this novel method is that the presence of an interface does not allow glissile dislocation segments to relax back as they are effectively pinned, thereby forming a dislocation forest in Fig. 1(b). Since the nucleated dislocations comprise inherent mobile segments, we anticipate them to respond actively during indentation. Yet, it remains an open question if the character of pre-existing dislocations influences the deformation behaviour, as the defect creation methods differ. This investigation is out of the scope of the present work. Nevertheless, we trust that our method mimics realistic dislocation interactions.

2.3. Position of indents

Fig. 1(b) shows a defective γ/γ' bi-crystal with a dense dislocation forest having a dislocation density in the order of $10^{16}/\text{m}^2$. While this numerical value is higher than observed in experiments, given the small indenter size ($R = 80$ Å) only a small fraction of defects will interact with the indenter stress field. This localized indenter interaction has often been overlooked in atomistic simulations, even though it has been shown experimentally that pop-ins could be triggered by activation of pre-existing dislocations under the indenter and if the size of the indenter is smaller than the dislocation spacing, a large spread of data is observed (Morris et al., 2011; Bei et al., 2016; Shim et al., 2008).

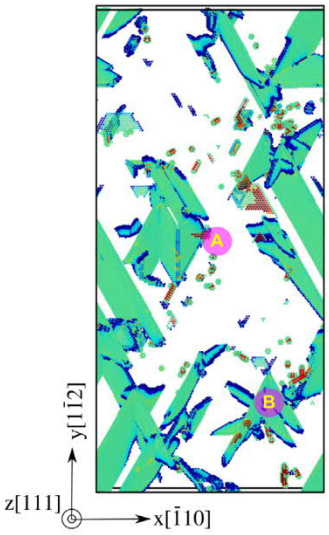

Fig. 2. γ layer showing defects as stacking faults with trailing or leading partials marked in blue and the stacking fault marked as green. The sample is indented upon at two positions A and B which are marked in pink labels.

Most previous studies (Alabd Alhafez et al., 2019; Lodes et al., 2011) drew conclusions by indenting only at a single location of the sample and applying continuum relations for indenter defect interactions. This essentially includes the hardening caused due to the overall dislocation density. However, dislocation density as a variable is only applicable when the complete sample is under deformation (Zepeda-Ruiz et al., 2017), where all dislocations are simultaneously exposed to some stress. In nanoscale indentations however, this condition is not met due to a localized stress field of the indenter and the probabilistic nature of finding defects under the indenter (Morris et al., 2011; Bei et al., 2008; Phani et al., 2013; Bei et al., 2016).

Alongside the above mentioned subtleties, the sample is extremely inhomogeneous, with interspersed hard and soft regions that should respond differently to indentation (Alabd Alhafez et al., 2019; Ukwatta and Achuthan, 2014; Salehinia and Bahr, 2012; Shankar et al., 2005; Bei et al., 2016; Wu et al., 2015; Shim et al., 2008; Patel and Lee, 2020). In our simulations a similar picture emerges when one examines the defects in γ layer as shown in Fig. 2, with various defects and stacking fault atoms clearly visible, that extend into the sample. Notably, there are interspersed defective and defect free regions in the sample which only allow for local interactions with the indenter.

Therefore, we refrain from classifying the sample using its dislocation density and indent at different locations of the *defective crystal* as shown in Fig. 2. In this study indentations were carried out at various locations, but for clarity in our discussions, we will only focus on the response of Position A and B shown in Fig. 2. We trust that the indentation responses of these strategic indent positions and ensuing discussions, covers the complete range of spectrum (Bei et al., 2016) with respect to indent positions. For example at Position A, the sample below the point of contact is defect free but has defects nearby. On the contrary, at Position B, the sample below the point of contact, has dislocations arranged in closed packed planes which emanate near the surface. We proceed with the anticipation that due to different arrangement of defects under the indenter the indentation response will change.

3. Results & discussion

3.1. Indentation response

The *force vs. displacement* curves of the defective bi-crystal at indented positions A and B are shown in Fig. 3a. For direct comparison the response of a defect free single-crystal is also shown, where the position of indent does not matter as there are no defects present. The deformation response of a defect free single crystal and defect free bi-crystal are similar (see Fig. A.11) and therefore, for the sake of a clear discussion we compare the response of defect free single-crystal only.

In a *defect free* crystal, Fig. 3a, the indenter undergoes an elastic contact with the sample until an indentation depth of ~ 8 Å which leads to a steady rise in force, followed by a sharp load drop from ~ 600 nN. This load drop corresponds to the nucleation of dislocations underneath the indenter, which spread into the crystal as the indenter drives into the sample. Thereafter, the force continues to rise intermittently, due to dislocation nucleation from the indented surface (Begau et al., 2011).

For a *defective* bi-crystal, Fig. 3a, the measured response at both indented positions, A and B, deviates substantially from that of a defect free crystal. At both these indented positions the elastic response shows only a marginal change, indicating that the presence of pre-existing defects barely alters elastic behaviour. This observation is consistent with previous studies (Lodes et al., 2011; Ukwatta and Achuthan, 2014; Alabd Alhafez et al., 2019). Beyond the elastic regime, we observe a distinct load drop, at a much lower indentation depth of ~ 4.5 Å, at both positions, A and B. Notably, the corresponding nucleation force is also significantly lower at

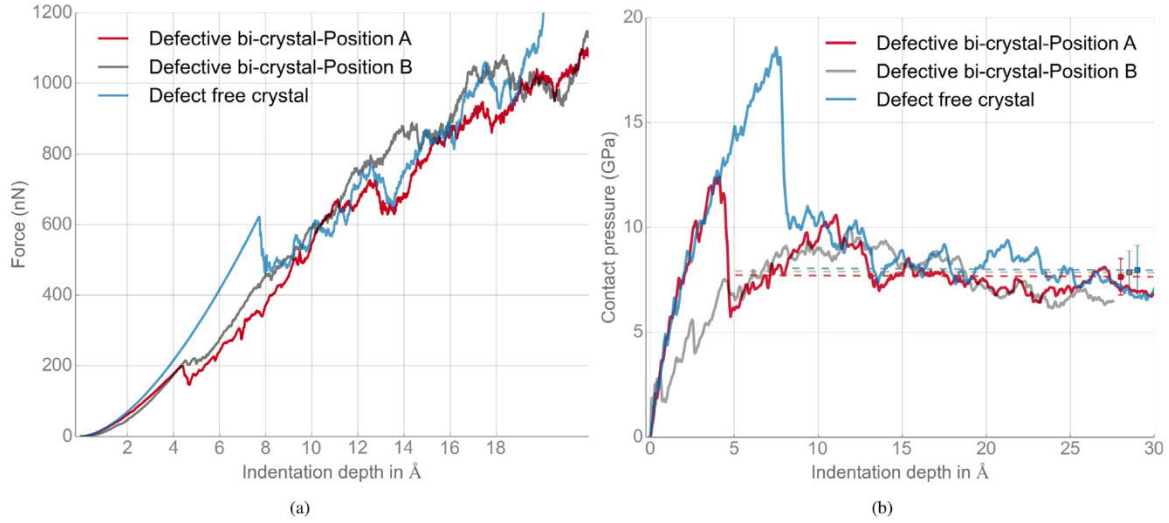

Fig. 3. Evolution of (a) Contact force and (b) Contact pressure with indentation depth. The average hardness is shown in (b) using dashed lines along with the calculated error bars. The average value and deviation are not positioned with respect to indentation depth but at a convenient location for clarity.

$\sim$ 200 nN, which is consistent with previous observations (Alabd Alhafez et al., 2019; Ukwatta and Achuthan, 2014; Salehinia and Bahr, 2012). After nucleation, the force continues to steadily rise with major and minor drops due to dislocation nucleation events.

Next, we consider the *contact pressure* evolution during indentation, shown in Fig. 3b. During elastic loading in a *defect free crystal*, the contact pressure rises steadily until there is dislocation nucleation at $\sim$ 18 GPa, which is manifested by a sharp drop. It is well recognized that the stress levels attained underneath the indenter, correspond to the theoretical shear strength of the material (Ziegenhain et al., 2015; Begau et al., 2011). The steep rise and drop of contact pressure occurs due to the release of elastic energy in dislocation nucleation and is perhaps a classic signature of defect free crystal (Begau et al., 2011). On subsequent loading, the contact pressure begins to attain a steady flow state. After the onset of plasticity the average value of the contact pressure is recorded as the crystal hardness, which is $\sim$ 8 GPa in this case.

For a defect free crystal, it is a common understanding, that after nucleation the contact pressure gradually attains a steady state without showing an intermittent monotonous rise. However, in a defective crystal, this cannot be the case, as we expect some work hardening due to dislocation interactions, which could not be seen before (Alabd Alhafez et al., 2019).

In a *defective* bi-crystal at *position A*, Fig. 3b, during elastic loading the contact pressure rises steadily until $\sim$ 5 Å, which is followed by a sharp drop. This sharp drop is akin to that of defect free crystal response, due to dislocation nucleation, but at a reduced contact pressure. After this pressure drop, we observe a remarkable monotonous rise from 5 Å to 11 Å depth and a second drop beyond $\sim$ 11 Å depth, before the pressure attains a steady state. The second monotonous rise in this case resembles a hardening stage, which was anticipated. The steady state average hardness is similar to that of a defect free crystal.

In a *defective crystal* at *position B*, Fig. 3b, the contact pressure during elastic loading deviates from a defect free crystal. The onset of nucleation occurs at $\sim$ 5 Å indentation depth at a far reduced contact pressure (lower than at Position A), but without a sharp rise and drop in contact-pressure. On further loading the contact-pressure rises steadily, until 11 Å, where it begins to converge. This response is peculiar, as it deviates from defect free crystal but also from Position A of the defective crystal. A steady convergence to average hardness shows that during elastic loading a rapid built up of pressure did not occur, but is dissipated due to the presence of pre-existing defects. This is analysed further in the following section.

So far, our results indicate that the deformation response of defective and defect free crystals are markedly different in the initial stages of indentation. Moreover, changing the position of indentation in a defective crystal itself can lead to significant changes in the indentation response, particularly during initial stages of loading. Also, we show that irrespective of the type of sample the contact pressure eventually converges to a steady value. To better understand the origins of this indentation response we discuss the corresponding plastic evolution stages during indentation, in the following section.

3.2. Plasticity evolution

Snapshots of defect evolution for a *defect free crystal* are shown in Fig. 4.

After elastic loading, incipient dislocations are nucleated under the indenter (below the surface) on {111} planes and grow, as can be seen in the snapshot for $D = 8.5$ Å. This nucleation stress is a measure of the theoretical shear strength of a crystal (Begau et al., 2011). After it has been reached, an avalanche of dislocations rapidly fills up the plastic zone to sustain plastic deformation by the indenter, which corresponds to a state after the stress drop in Fig. 3b. Now, dislocations can easily propagate as shown for D = 9.5–10.5 Å, where a distinct prismatic loop is in process of being detached from the surface. It is typical of such prismatic

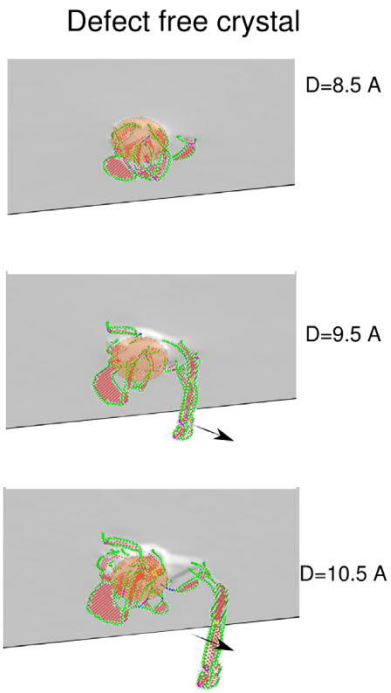

Fig. 4. Snapshots of dislocation nucleation during indentation in a defect free crystal. Only defect atoms are visible which are filtered according to common neighbour analysis and red atoms lie in stacking faults. Alongside, the dislocation partials are outlined in green. The grey region denotes the surface, and the camera views the indentation from below the sample, such that the indenter is hidden by the grey surface. To show the position of the indenter, its initial contact position is marked by a pale pink disk, overlayed on the grey surface. The process of dislocation of evolution can also be seen from Movie 1 (Supplementary 1).

loops to form on {111} planes and detach (Begau et al., 2011; Lee et al., 2020), while contact pressure converges to a lower stress as defects grow in size. Alongside, dislocations are constantly nucleated near the surface steps (Zimmerman et al., 2001) and the stresses necessary to drive them are still in order of the theoretical shear strength of the material (Begau et al., 2011). Thus both processes of nucleation and growth can occur simultaneously as the indenter drives further into the sample.

Snapshots of defect evolution in a *defective* bi-crystal, indented at *position A* are shown in Fig. 5. For clarity, only a small section of the sample under the indenter is shown. The state of the sample before indentation, at $D = 0$ Å, shows pre-existing dislocation partials which terminate at the surface. Alongside, a peach coloured disk shows the targeted indentation position. This contact position is strategic, as it lies near a dislocation partial which extends into the sample, but the point of contact itself is free of any defects. Upon indentation, defects are nucleated under the point of contact at ~ 5 Å indentation depth (not shown) and grow in size as shown in Fig. 5, at $D = 6.05$ Å. This process is similar to nucleation in a defect free crystal in Fig. 5, which leads to an elastic contact and corresponding sharp pressure drop in Fig. 3b. Even though the nucleation stress for defective crystal is lower than for a defect free crystal, there are similarities in the nucleation behaviour and contact pressure response. This shows that the indenter detects only a very local region of the sample, and in this case, manifests a defect free crystal like behaviour during nucleation, at a reduced nucleation stress. The above behaviour is also akin to nucleation dominated plasticity using nanoscaled spherical indenters, which show homogeneous nucleation of dislocations at close to theoretical strength (Shim et al., 2008; Bei et al., 2016).

As the nucleated defects grow in size, they begin to interact with pre-existing defects. For instance, as shown in Fig. 5, $D = 9.05$ Å, a nucleated dislocation lies on the same plane as a pre-existing dislocation ribbon. As the indenter drives further, $D = 10.05$–12.05 Å, it pushes this dislocation into the sample and is impeded by a pre-existing dislocation ribbon. This process is akin to a pile up phenomenon and $D = 12.05$ Å shows how the pre-existing ribbon shrinks.

Interestingly, in snapshots from $D = 6.05$–12.05 Å, the plastic strain is carried primarily by this one propagating dislocation, as there is negligible dislocation activity otherwise. Thus the contact pressure response should manifest this local phenomenon and is a key observation, as the defect interactions coincides with a rise in contact pressure in Fig. 3b, from $D = 5$ Å to $D \sim 12$ Å. Therefore, the apparent increase in contact pressure is a direct consequence of defect interactions. However, on further loading these interactions do not persist and an intense dislocation surge is observed, but distinctly away from the pre-existing dislocations towards the defect free region, as shown in Fig. 5, $D = 13.05$ Å. This later stage evolution of defects, away from pre-existing defects, was also observed previously (Alabd Alhafez et al., 2019). Overall, the results show an increased sensitivity to defect interactions during initial stages of indentation but the interactions slowly subside as plasticity is diverted into defect free regions.

Snapshots of defect evolution in a *defective* bi-crystal, indented at *position B*, are shown in Fig. 6. As shown in Fig. 6, at $D = 0$ Å, the indenter position lies directly above the pre-existing partials near the surface, nucleated along two intersecting closed packed (111) planes. This achieves a strategic purpose to verify if the presence of aligned pre-existing defects have an influence on indentation

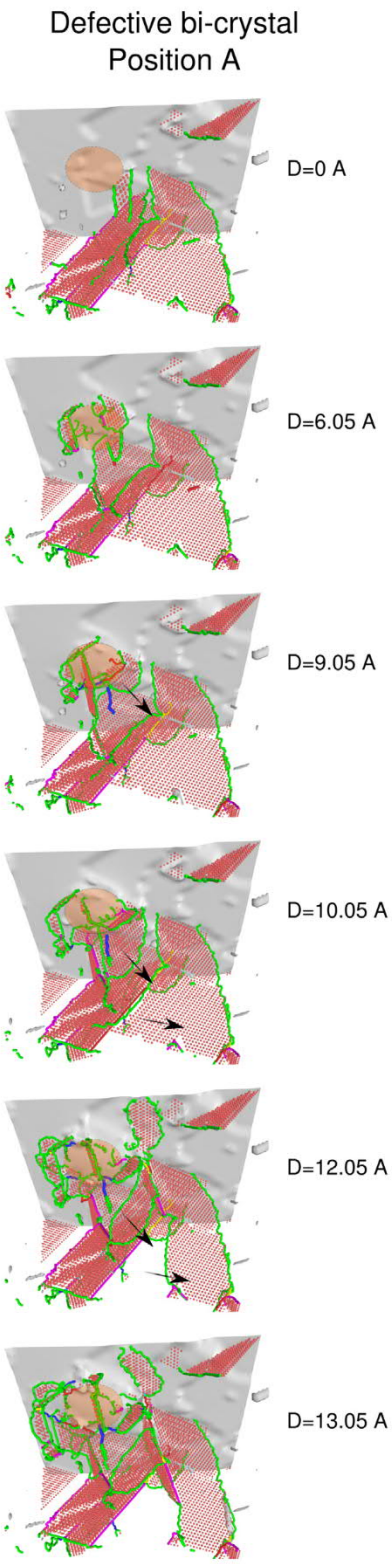

Fig. 5. Snapshots of dislocation nucleation during indentation for a *defective* bi-crystal indented at *position A*. The colour scheme is same as in Fig. 4. Black arrows denote the direction of dislocation propagation. At $D = 10.05$ Å and $D = 12.05$ Å a black arrow shows how a pre-existing partial contracts as a dislocation propagates into the sample. The process can also be seen from Movie 2 (Supplementary 1).

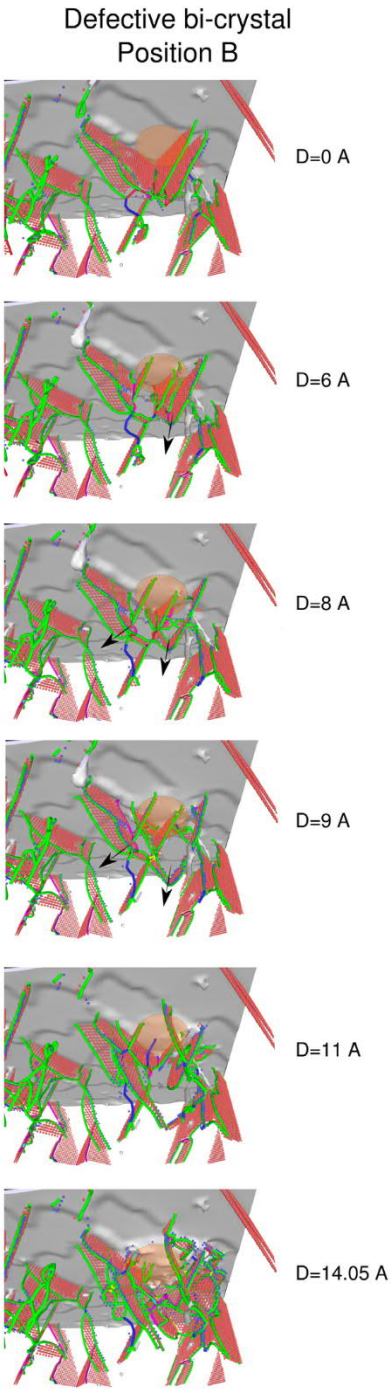

Fig. 6. Snapshots of dislocation nucleation during indentation for a *defective* bi-crystal indented at *position B*. Black arrows depict the direction of seamless growth of pre-existing partials into the sample. $D = 14.05$ Å shows new dislocation nucleation near the surface. The process of seamless growth can also be seen from Movie 3 (Supplementary 1).

response and if nucleation of new defects can be suppressed. During indentation the elastic regime remains unaffected, but plasticity proceeds by some rearrangement of partials directly underneath the indenter at $D = 6$ Å. This way the strain is accommodated by local rearrangement and new defect nucleation is suppressed. Instead, pre-existing partials under the indenter rearrange and are driven into the sample, as seen for $D = 6$ Å to $D = 11$ Å. Notice how this behaviour seamlessly allows prismatic dislocations to be driven into the sample in the Movie 3 (Supplementary 1).

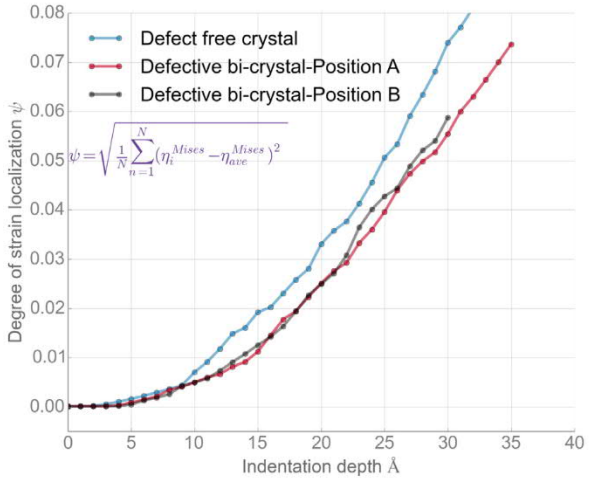

Fig. 7. Evolution of strain localization parameter ψ with indentation depth. ψ measures how strain is localized or spread out,under the indenter.

A striking consequence of the above behaviour is an altered contact pressure response, shown in Fig. 3b, which gradually converges without abrupt load bursts. Moreover, seamless defect nucleation prevents a rapid rise and drop of contact-pressure, in contrast to previous cases. The mechanism of growth of pre-existing partials is peculiar, as such a behaviour has not been observed hitherto in MD simulations, yet has been expected (Alabd Alhafez et al., 2019; Lodes et al., 2011; Shankar et al., 2005; Ukwatta and Achuthan, 2014). In fact, in-situ TEM investigations using a nanoscale indenter clearly show pre-existing dislocations detaching from the indented surface (Bufford et al., 2014), which corroborate our observations. On further indentation, the mechanism transitions from seamless growth of dislocations to a rapid surge of newly nucleated dislocations, as shown in Fig. 6, at $D = 14.05$ Å. Note, that this is the first instance of new dislocations being nucleated, primarily from the surface.

To summarize, the above described defect evolution stages show that, indeed, pre-existing defects and their interactions influence the measured contact-pressure during initial stages of loading. Thus, pre-existing dislocations can influence the measured hardness. Consequently, indenting at different positions of the sample manifests a contrasting contact-pressure response, which we correlate to different interaction mechanisms. Namely, local pile up and seamless propagation of dislocations. During later stages of loading the contact pressure converges to an average value.

To this end snapshots in Figs. 5, 4, 6 provide a direct evidence of dislocation evolution, which we correlate to indentation response, but these effects remain to be quantified. Therefore, in the next section we compare and contrast the defect evolution stages using quantifiable parameters.

3.3. Measuring localization of plasticity

The extent and evolution of the plastic zone for the same indentation depth is different for defective and defect free samples. Since the movement of dislocations, nucleated from the indenter, is impeded due to pre-existing defects, we may be tempted to believe that plasticity gets more localized in a defective sample as compared to defect free crystal. However, the snapshots show only a small region under the indenter and do not provide enough information about overall strain accommodation by pre-existing defects. Moreover, a direct comparison of plasticity localization is not trivial due to different initial defect densities in defective and defect free sample.

To quantify plasticity evolution we consider two quantities — a strain localization parameter and the dislocation line length. The *strain localization parameter* (SLP) is a measure of indenter induced plasticity only and is calculated as

$$\psi = \sqrt{\frac{1}{N}\sum_{n=1}^{N}(\eta_i^{Mises} - \eta_{ave}^{Mises})^2}$$

at successive indentation depths (Cheng et al., 2009). η_i^{Mises} is calculated with respect to a reference configuration and η_{ave}^{Mises} is the average of von Mises strain of all atoms; N is the total number of atoms. Thus, ψ evaluates the deviation of strain distribution and encompasses both elastic and plastic deformation of the indenter. A larger ψ will indicate a more localized deformation under the indenter. The evolution of SLP with indentation depth is shown in Fig. 7. Simultaneously, the *dislocation line length* is calculated over a slab of γ, which is 11 nm thick for both defective and defect free crystals. Since the starting dislocation length for the two samples is different, we employ two axes in Fig. 8 to simultaneously compare dislocation evolution.

For a *defect free crystal*, during the elastic regime, ψ grows gradually as the elastic strain gets homogeneously distributed. At the onset of nucleation we observe a sharp rise from ~ 8 Å depth. This is understandable, as plasticity gets largely localized under the indenter, also visible in snapshots in Fig. 5. Thereafter as the indentation depth increases, ψ progressively increases due to

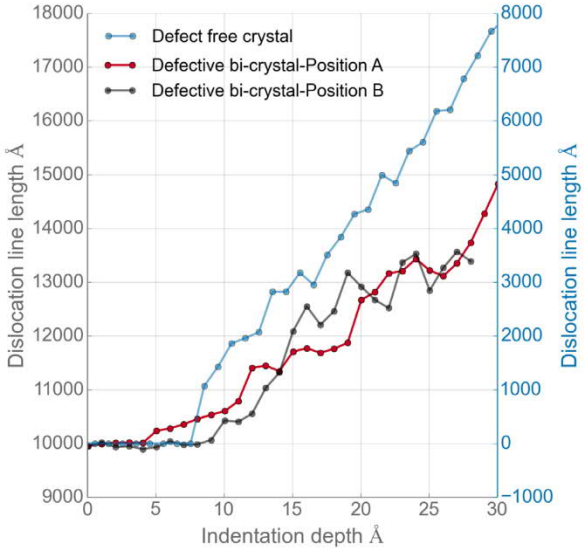

Fig. 8. Dislocation line length evolution with indentation depth for various samples. The initial line length for a *defective* bi-crystal is finite, whereas in a *defect free* crystal it is 0 Å, which is compared using a blue axis on the right.

continuous localization of deformation. The nature of rise in ψ is also congruous with the dislocation line length evolution in Fig. 8. In a *defect free* crystal there is no change in dislocation length during elastic loading, due to unavailability of dislocations. Upon nucleation at $\sim$ 8 Å depth, a rapid burst of dislocation nucleation occurs which leads to a precipitous rise in dislocation length. This precipitous rise is monotonous due to continuous nucleation and coincides with the observed avalanche of dislocations in Section 3.2, which is a characteristic of defect free crystal, Fig. 4.

For *defective* bi-crystal during elastic regime, ψ rises gradually but nucleation already occurs at $\sim$ 5 Å for both Positions A and B. Yet, ψ rises gradually(compared to defect free crystal), indicating that deformation gets distributed in the sample. This deformation is carried by pre-existing dislocations in the sample which creates an offset in ψ between defect free and defective sample. The gradual rise of ψ continues until $\sim$ 15 Å where the slope changes and we observe a rapid rise, similar to the slope of the defect free crystal. Remarkably, $\sim$ 15 Å is also the depth at which contact-pressure starts converging in Fig. 3b and initial fluctuations cease.

To distinguish the differences in plasticity evolution in a defective crystal we see the *dislocation length* evolution in Fig. 8. For a *defective* bi-crystal, *position A*, the dislocation length starts to increases at 5 Å indentation depth due to nucleation. However, this increase is very gradual compared to a defect free crystal, which coincides with the dislocation interactions after nucleation, described in Fig. 5. This behaviour indicates that deformation of the indenter is accommodated by pre-existing defects, instead of major nucleations. At further indentation depth, $\sim$ 12 Å, we observe a small rise in dislocation length which coincides with a rapid burst of new defects under the indenter. After which the dislocation length plateaus again, until $\sim$ 19 Å, where another rapid rise is observed. Overall, the dislocation length evolution evolves in intermittent surges that is not monotonous which is indicative of nucleation events and subsequent interaction with pre-existing defects.

Note that, we were only able to isolate one pile-up phenomenon distinctly in Fig. 5 and correlate it to contact pressure and dislocation line length change, however, more such events can occur upon indentation which are difficult to identify due to large number of defects. Yet, the nature of the dislocation length evolution provides a reasonable estimation of the underlying interactions.

For a *defective crystal* at *position B*, no change in dislocation line length is observed even after the onset of plasticity at $\sim$ 5 Å. Which also coincides with the seamless growth of defects under the indenter shown in Fig. 6. Clearly, a seamless growth manifests as only a marginal change in dislocation length, which only begins to rise at $\sim$ 11 Å depth and coincides with the onset of new dislocations in Fig. 6. Thereafter, the dislocation length evolves in intermittent surges.

Overall, using the above analysis we show how pre-existing defects play a crucial role by correlating indenter response and defect evolution to measurable quantities. The evolution of SLP ψ shows how efficiently deformation is transmitted, while dislocation length evolution provides a quantifiable basis to observations in Section 3.2. Also, it reinforces the idea that the nature and position of defects in the sample can drastically change the indentation response.

However, one observation which consistently occurs in our results is a transition in deformation behaviour at $\sim$ 15 Å. Fig. 3b shows a contact-pressure convergence at this depth for all samples. Simultaneously, defect evolution shows a transition in Section 3.2, to a surge of new dislocations under the indenter. Even SLP ψ, shows a marked change of slope at $\sim$ 15 Å. We unravel the origins of this observation in the next section.

3.4. Influence of indenter size

Here we address a pertinent question that may have arisen in the readers mind, that even though initial defect interactions from pre-existing dislocations influence indenter response, *why does the contact pressures converge?* Not only for the types of samples

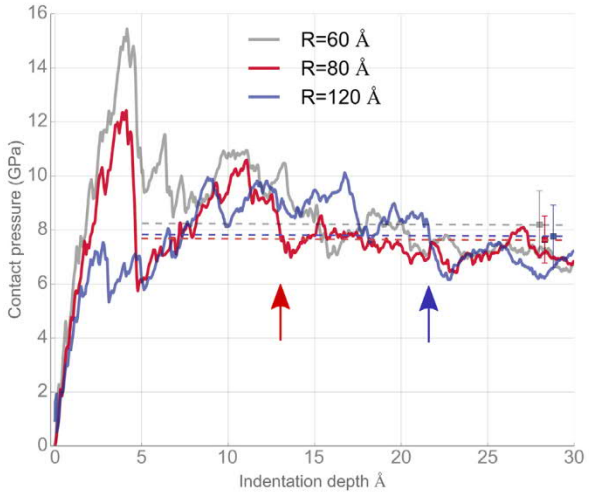

Fig. 9. Contact pressure evolution with indentation for increasing indenter radii. $R = 80$ Å pertains to all previously shown results. Here the average hardness is marked with dashed lines along with its deviation on the right. The coloured arrows indicate the depth at which contact pressure converges for different indenter radii.

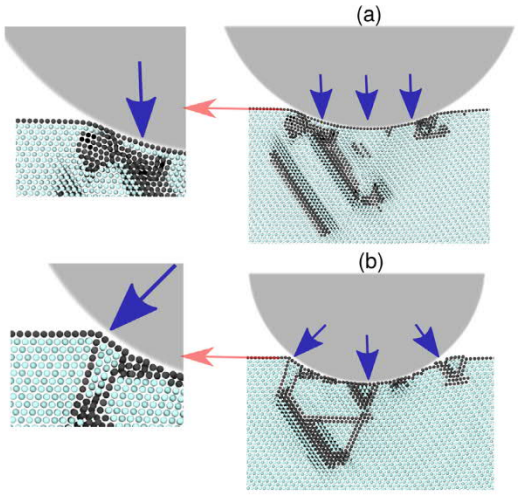

Fig. 10. Curvature effect for (a) R = 12 nm (b) R = 8 nm indenter radii. The contact angle θ increases with decreasing indenter radius.

used-defective or defect free, but also for different indentation positions in Fig. 3b. The transition at approximately 15 Å indentation depth in Fig. 3b, is reflected in the analysis, Section 3.3, as well. At this stage, in a defective sample, the mechanism shifts from dislocation interactions to a burst of new nucleations under the indenter. This phenomenon depends on indentation depth which provides a clue that its origins could be geometric in nature. In which case, we anticipate the indenter size to be this geometric factor.

To test this, we carry out indentations using varying indenter sizes on a defective crystal at *Position A* shown in Fig. 2. In Fig. 9 we show the contact pressure evolution curves for three indenter radii, increasing from $R = 60$ Å to $R = 120$ Å where $R = 80$ Å was used for our previous results.

From Fig. 9 we see that for a larger indenter, $R = 120$ Å, the critical stress of nucleation is substantially lower than for $R = 80$ Å. For $R = 60$ Å it is remarkably higher, which establishes a trend. This systematic decrease in nucleation stress with increase in indenter size implies that the indenter with $R = 60$ Å interacts very locally with the sample (which is defect free), such that the response is akin to a defect free crystal. This is evident from the nucleation stress being closer to that of a defect free crystal, ~ 18 GPa, and a sharp drop, which is a characteristic of defect free crystal. Thus for a small indenter ($R = 60$ Å) the indentation response is highly sensitive to the position of indentation. In contrast, for indenter sizes $R = 80$ Å and $R = 120$ Å, the contact encompasses a larger area of the sample and enables the indenter to interact with the stress fields of many sample defects, which leads to a systematic decrease in nucleation stress. Thus, for a large indenter size a more averaged response of the sample defects is detected which is less sensitive to the position of indent.

This behaviour attests to the experimental observations (Shim et al., 2008; Bei et al., 2016), which show that theoretical strength is achieved for smaller indenters while for larger indenters pop-in can occur at a much lower applied stress. This indentation size effect is remarkably present even at atomic length scales with the effect of "smaller is stronger", albeit with respect to indenter size. It also explains why there is a large variation in cumulative probability of pop-ins (Morris et al., 2011) as the indenter size systematically decreases. Our results indicate that this variability arises due to the changing nature of pre-existing dislocations under the indenter. Specially, if the indenter impinges on a defect free part of specimen, the behaviour is nucleation dominated and results in high indentation stress. The transition from nucleation dominated to dislocation activated plasticity (Shim et al., 2008; Bei et al., 2016) is also evident as the indenter size increases

So far our results show that for $R = 60$ Å the indentation response is akin to defect free crystal while for $R = 80, 120$ Å pre-existing defects play a significant role in indentation response. Yet the contact-pressure converges for all indenter radii. For $R = 80$ Å, the contact-pressure remains higher than the average until ~ 15 Å depth, where it begins to converge. Similarly, for $R = 120$ Å, the contact-pressure rises higher than even the nucleation stress and stays higher than average until ~ 22 Å, where it begins to converge. This is shown by coloured arrows in Fig. 9. Clearly, the depth of convergence increases as indenter radius increases. Also, the portion of the curve higher than the average hardness is more for $R = 120$ Å than $R = 80$ Å which shows that by using a larger indenter, dislocation interactions are manifested on the contact-pressure curve for a greater indentation depth.

This phenomenon can be understood, if we recall that we observe in our simulations, that the approximate depth of convergence coincides with the nucleation of fresh defects near the indenter, Section 3.2. These new nucleation events originate around the circumference of the indenter contact circle which in turn depends upon the indenter radius.

We show in Fig. 10 the state of the sample (defect free crystal) in contact with indenter (a) with $R = 120$ Å and (b) with $R = 80$ Å, for the same indentation depth of $D = 17.5$ Å. For $R = 120$ Å indenter radius, the sample defects have already evolved but the contact surface is still smooth without any steps or kinks. At this stage a relatively flat part of the indenter is in contact and the defects continue to propagate/nucleate in the bulk sample to accommodate deformation. In doing so, the underlying dislocation interactions get clearly manifested in the contact-pressure measurement. In contrast, for $R = 80$ Å, though the sample defects have evolved, the surface shows sharp kinks due to the nucleation of defects from the surface. At this stage, the indenter is driven so deep that its curvature must be accommodated by circumferential dislocations which are geometrically necessary (Nix and Gao, 1998; Dahlberg et al., 2014; Gao and Huang, 2003; Swadener et al., 2002; Liu et al., 2019). However, now the contact-pressure is predominantly influenced by surface nucleations which occur at lower stress (Kelchner et al., 1998). Thus the contact-pressure no longer factors the influence of sample defects.

Thus convergence at some indentation depth in Fig. 9 is a result of curvature accommodation near the contact surface. For a large indenter ($R = 120$ Å), the curvature accommodation depth is delayed as compared to a smaller indenter ($R = 80$ Å). Until this depth is reached, the indenter continues to manifest the indenter defect interactions in contact-pressure, which remain higher than average. For a small indenter ($R = 60$ Å) the curvature effect dominates immediately after nucleation, due to which a steady convergence is observed. This curvature effect is notably also visible in nanoscale experimental investigation (Bufford et al., 2014; Engels et al., 2018) and is intuitively expected. Especially in in-situ experiments (Bufford et al., 2014) a transition from dislocation activated plasticity to nucleation dominated plasticity is observed to accommodate the indenter curvature. It also indicates that the classical idea of GNDs (Nix and Gao, 1998) holds true for larger indentation depths, where the indenter curvature has been accommodated at the surface but not for shallow indentation depths (with respect to indenter).

Thus, the effect of indenter radius is crucial in the overall understanding of indentation with pre-existing defects. We have shown that by changing indenter radius we can vary its sensitivity to effectively detect sample defects such that for a large indenter the interactions could be felt for a larger depth. Overall, the implication is that given a large simulation box with a considerably large indenter, pre-existing defects will have a profound influence on the measured hardness of a crystal. We also trust that the systematic trend of detecting higher than average hardness can be extrapolated to larger length scales, which corroborates with the understanding of Taylor's hardening (Nix and Gao, 1998) that includes the dislocation density instead of dislocation position.

4. Conclusions

The influence of pre-existing defects on nanoindentation is studied using TiAl bi-layers, employing a novel dislocation population technique with misfit dislocations at a γ-pseudo twin interface. Indentation is carried on defective and defect free samples, where a defective bi-crystal is considered as a heterogeneous sample and is indented at two different positions.

The indentation response reveals stark differences between defective and defect free samples. Moreover, the response is markedly different at different indented positions in a defective sample, which affirms our initial assumption to treat the sample as inhomogeneous. Different responses in contact-pressure are directly correlated to indenter defect interactions, namely pile-ups and seamless growth mechanisms. We show that the plastic strain can efficiently be distributed amongst crystal defects. Also, dislocation interactions manifest themselves in dislocation length evolution. Finally, we observe that contact pressure in large indenters can remain higher than average for an extended depth. An eventual convergence to a lower value is a result of curvature accommodation at the surface.

Thus pre-existing dislocations can markedly affect the calculated hardness particularly during initial indentation depths, and care should be taken in choosing indented positions. A hardening behaviour should be expected as long as the indenter size and simulations volumes are substantially large. While indenting on defect free crystals may provide valuable insights about theoretical limits of a crystal, indenting on defective crystals encompasses information about indenter-defect and defect–defect interactions. This insight is valuable as dislocation interactions with microstructural features such as twin boundaries, grain boundaries and other dislocations can be studied. Our results also conform to experimental investigations in the literature and reinforce the notion that large scale atomistic simulations can be used to simulate realistic defect interactions and micro structures. We trust our results will be valuable for numerous atomistic simulations with pre-existing defects in the future and for analysis of in-situ TEM data.

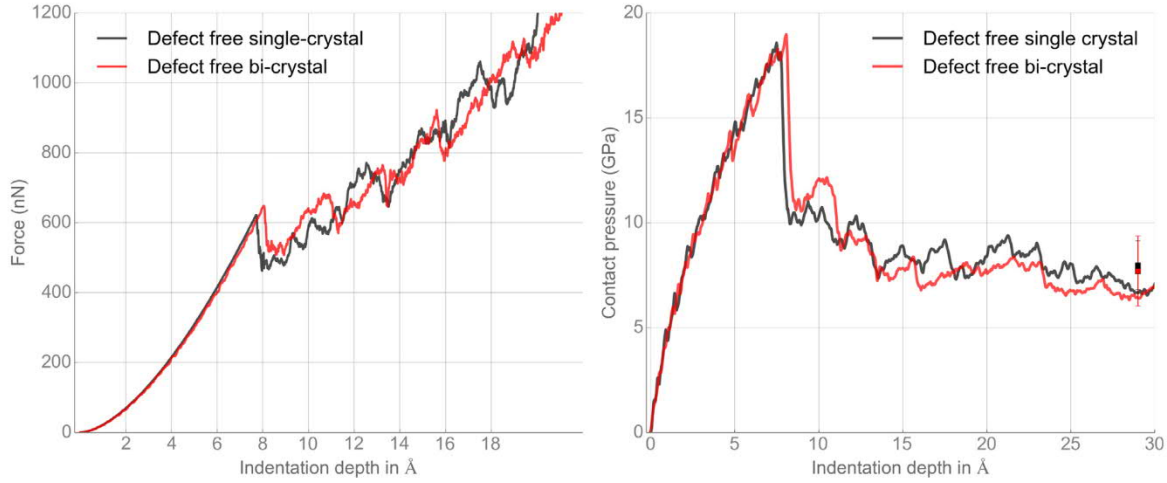

Fig. A.11. Evolution of (a) Contact force and (b) Contact pressure for defect free *single* crystal and defect free *bi-crystal* crystal.

Declaration of competing interest

The authors declare that they have no known competing financial interests or personal relationships that could have appeared to influence the work reported in this paper.

Acknowledgements

This work was supported by the German Science Foundation (DFG) under grant number 404541620. A.C. acknowledges support from the International Max Planck Research School for Surface and Interface Engineering (IMPRS-SurMat), Germany. G.D. acknowledges the ERC Advanced Grant GB-CORRELATE, Germany (Grant No. 787446).

Appendix A

Comparison of indentation response of defect free single and bi-crystal in Fig. A.11 shows similar behaviour. Thus the presence of a bi-crystal and misfit dislocations do not have an influence on the indentation response for the given layer thickness.

Appendix B. Supplementary data

Supplementary material related to this article can be found online at https://doi.org/10.1016/j.jmps.2021.104511. Three movies are provided as supplementary data that pertain to Figs. 4–6.

References

Alabd Alhafez, I., Ruestes, C.J., Bringa, E.M., Urbassek, H.M., 2019. Influence of pre-existing plasticity on nanoindentation – an atomistic analysis of the dislocation fields produced. J. Mech. Phys. Solids 132, 103674.
Appel, F., Paul, J.D.H., Oehering, M., 2011. Gamma Titanium Aluminide Alloys: Science and Technology. Wiley-VCH Verlag GmbH & Co. KGaA.
Barnoush, A., 2012. Correlation between dislocation density and nanomechanical response during nanoindentation. Acta Mater. 60 (3), 1268–1277.
Begau, C., Hartmaier, A., George, E.P., Pharr, G.M., 2011. Atomistic processes of dislocation generation and plastic deformation during nanoindentation. Acta Mater. 59 (3), 934–942.
Bei, H., Gao, Y.F., Shim, S., George, E.P., Pharr, G.M., 2008. Strength differences arising from homogeneous versus heterogeneous dislocation nucleation. Phys. Rev. B 77 (6), 2–5.
Bei, H., Xia, Y.Z., Barabash, R.I., Gao, Y.F., 2016. A tale of two mechanisms: Strain-softening versus strain-hardening in single crystals under small stressed volumes. Scr. Mater. 110, 48–52.
Bufford, D., Liu, Y., Wang, J., Wang, H., Zhang, X., 2014. In situ nanoindentation study on plasticity and work hardening in aluminium with incoherent twin boundaries. Nature Commun. 5 (1), 4864.
Catoor, D., Gao, Y.F., Geng, J., Prasad, M.J., Herbert, E.G., Kumar, K.S., Pharr, G.M., George, E.P., 2013. Incipient plasticity and deformation mechanisms in single-crystal mg during spherical nanoindentation. Acta Mater. 61 (8), 2953–2965.
Chauniyal, A., Janisch, R., 2020. Influence of lattice misfit on the deformation behaviour of $\alpha 2/\gamma$ lamellae in tial alloys. Mater. Sci. Eng. A 796.
Cheng, Y.Q., Cao, a.J., Ma, E., 2009. Correlation between the elastic modulus and the intrinsic plastic behavior of metallic glasses: The roles of atomic configuration and alloy composition. Acta Mater. 57 (11), 3253–3267.
Choi, I.C., Kim, Y.J., Wang, Y.M., Ramamurty, U., Jang, J.I., 2013. Nanoindentation behavior of nanotwinned Cu: Influence of indenter angle on hardness, strain rate sensitivity and activation volume. Acta Mater. 61 (19), 7313–7323.

Dahlberg, C.F., Saito, Y., Öztop, M.S., Kysar, J.W., 2014. Geometrically necessary dislocation density measurements associated with different angles of indentations. Int. J. Plast. 54, 81–95.
Derlet, P.M., Maaß, R., 2016. Critical stress statistics and a fold catastrophe in intermittent crystal plasticity. Phys. Rev. E 94 (3), 1–11.
Engels, J.K., Gao, S., Amin, W., Biswas, A., Kostka, A., Vajragupta, N., Hartmaier, A., 2018. Indentation size effects in spherical nanoindentation analyzed by experiment and non-local crystal plasticity. Materialia 3 (September), 21–30.
Fischer-Cripps, A., Nicholson, D., 2004. Nanoindentation. Mechanical engineering series. Appl. Mech. Rev. 57 (2), B12.
Gao, H., Huang, Y., 2003. Geometrically necessary dislocation and size-dependent plasticity. Scr. Mater. 48 (2), 113–118.
Jin, K., Xia, Y., Crespillo, M., Xue, H., Zhang, Y., Gao, Y.F., Bei, H., 2018. Quantifying early stage irradiation damage from nanoindentation pop-in tests. Scr. Mater. 157, 49–53.
Kelchner, C.L., Plimpton, S.J., Hamilton, J.C., 1998. Dislocation nucleation and defect structure during surface indentation. Phys. Rev. B 58 (17), 58.
Ko, W.S., Stukowski, A., Hadian, R., Nematollahi, A., Jeon, J.B., Choi, W.S., Dehm, G., Neugebauer, J., Kirchlechner, C., Grabowski, B., 2020. Atomistic deformation behavior of single and twin crystalline Cu nanopillars with preexisting dislocations. Acta Mater. 197, 54–68.
Lee, S., Vaid, A., Im, J., Kim, B., Prakash, A., Guénolé, J., Kiener, D., Bitzek, E., Oh, S.H., 2020. In-situ observation of the initiation of plasticity by nucleation of prismatic dislocation loops. Nature Commun. 11 (1), 1–11.
Liu, W., Chen, L., Cheng, Y., Yu, L., Yi, X., Gao, H., Duan, H., 2019. Model of nanoindentation size effect incorporating the role of elastic deformation. J. Mech. Phys. Solids 126, 245–255.
Liu, Y., Jian, J., Chen, Y., Wang, H., Zhang, X., 2014. Plasticity and ultra-low stress induced twin boundary migration in nanotwinned Cu by in situ nanoindentation studies. Appl. Phys. Lett. 104 (23).
Lodes, M.A., Hartmaier, A., Göken, M., Durst, K., 2011. Influence of dislocation density on the pop-in behavior and indentation size effect in CaF2 single crystals: Experiments and molecular dynamics simulations. Acta Mater. 59 (11), 4264–4273.
Minor, A.M., Syed Asif, S.A., Shan, Z., Stach, E.A., Cyrankowski, E., Wyrobek, T.J., Warren, O.L., 2006. A new view of the onset of plasticity during the nanoindentation of aluminium. Nature Mater. 5 (9), 697–702.
Montagne, A., Audurier, V., Tromas, C., 2013. Influence of pre-existing dislocations on the pop-in phenomenon during nanoindentation in MgO. Acta Mater. 61 (13), 4778–4786.
Morris, J.R., Bei, H., Pharr, G.M., George, E.P., 2011. Size effects and stochastic behavior of nanoindentation pop in. Phys. Rev. Lett. 106 (16), 1–4.
Morris, J.W., Jin, M., Minor, A.M., 2007. In situ studies of the transmission of strain across grain boundaries. Mater. Sci. Eng. A 462 (1–2), 412–417.
Nair, A.K., Parker, E., Gaudreau, P., Farkas, D., Kriz, R.D., 2008. Size effects in indentation response of thin films at the nanoscale: A molecular dynamics study. Int. J. Plast. 24 (11), 2016–2031.
Nix, W.D., Gao, H., 1998. Indentation size effects in crystalline materials: A law for strain gradient plasticity. J. Mech. Phys. Solids 46 (3), 411–425.
Njeim, E.K., Bahr, D.F., 2010. Atomistic simulations of nanoindentation in the presence of vacancies. Scr. Mater. 62 (8), 598–601.
Ohmura, T., Minor, A.M., Stach, E.A., Morris, J.W., 2004. Dislocation-grain boundary interactions in martensitic steel observed through in situ nanoindentation in a transmission electron microscope. J. Mater. Res. 19 (12), 3626–3632.
Oliver, W.C., Pharr, G.M., 1992. An improved technique for determining hardness and elastic modulus using load and displacement sensing indentation experiments. J. Mater. Res. 7 (6), 1564–1583.
Patel, H.D., Lee, S.W., 2020. Spherical nanoindentation on tungsten single crystal: The transition from source-controlled plasticity to bulk plasticity. Scr. Mater. 175, 16–19.
Phani, P.S., Johanns, K.E., George, E.P., Pharr, G.M., 2013. A stochastic model for the size dependence of spherical indentation pop-in. J. Mater. Res. 28 (19), 2728–2739.
Pharr, G.M., Herbert, E.G., Gao, Y., 2010. The indentation size effect: A critical examination of experimental observations and mechanistic interpretations. Annu. Rev. Mater. Res. 40, 271–292.
Plimpton, S., 1995. Fast parallel algorithms for short – Range molecular dynamics. J. Comput. Phys. 117 (June 1994), 1–19.
Salehinia, I., Bahr, D.F., 2012. The impact of a variety of point defects on the inception of plastic deformation in dislocation-free metals. Scr. Mater. 66 (6), 339–342.
Salehinia, I., Wang, J., Bahr, D.F., Zbib, H.M., 2014. Molecular dynamics simulations of plastic deformation in Nb/NbC multilayers. Int. J. Plast. 59, 119–132.
Shankar, M.R., King, A.H., Chandrasekar, S., 2005. Dislocation-indenter interaction in nanoindentation. J. Appl. Phys. 98 (2), 023502.
Shim, S., Bei, H., George, E.P., Pharr, G.M., 2008. A different type of indentation size effect. Scr. Mater. 59 (10), 1095–1098.
Stukowski, A., Albe, K., 2010. Dislocation detection algorithm for atomistic simulations. Modelling Simulation Mater. Sci. Eng. 18 (2), 015012.
Stukowski, A., Bulatov, V.V., Arsenlis, A., 2012. Automated identification and indexing of dislocations in crystal interfaces. Modelling Simulation Mater. Sci. Eng. 20 (8), 085007.
Swadener, J.G., George, E.P., Pharr, G.M., 2002. The correlation of the indentation size effect measured with indenters of various shapes. J. Mech. Phys. Solids 50 (4), 681–694.
Taylor, G.I., 1938. Plastic strain in metals. J. Inst. Met. 62, 307–324.
Ukwatta, A., Achuthan, A., 2014. A molecular dynamics (MD) simulation study to investigate the role of existing dislocations on the incipient plasticity under nanoindentation. Comput. Mater. Sci. 91, 329–338.
Voyiadjis, G.Z., Yaghoobi, M., 2017. Review of nanoindentation size effect: Experiments and atomistic simulation. Crystals 7 (10), 8–10.
Wu, D., Morris, J.R., Nieh, T.G., 2015. Effect of tip radius on the incipient plasticity of chromium studied by nanoindentation. Scr. Mater. 94, 52–55.
Xia, Y., Gao, Y., Pharr, G.M., Bei, H., 2016. Single versus successive pop-in modes in nanoindentation tests of single crystals. J. Mater. Res. 31 (14), 2065–2075.
Zepeda-Ruiz, L.A., Stukowski, A., Oppelstrup, T., Bulatov, V.V., 2017. Probing the limits of metal plasticity with molecular dynamics simulations. Nature 550 (7677), 492–495.
Zhang, R.F., Wang, J., Beyerlein, I.J., Misra, A., Germann, T.C., 2012. Atomic-scale study of nucleation of dislocations from fcc-bcc interfaces. Acta Mater. 60 (6–7), 2855–2865.
Ziegenhain, G., Urbassek, H.M., Hartmaier, A., 2015. Influence of crystal anisotropy on elastic deformation and onset of plasticity in nanoindentation: A simulational study. J. Appl. Phys. 107 (2010), 061807.
Zimmerman, J.A., Bammann, D.J., Gao, H., 2009. Deformation gradients for continuum mechanical analysis of atomistic simulations. Int. J. Solids Struct. 46 (2), 238–253.
Zimmerman, J.A., Kelchner, C.L., Klein, P.A., Hamilton, J.C., Foiles, S.M., 2001. Surface step effects on nanoindentation. Phys. Rev. Lett. 87 (16), 14–17.
Zope, R.R., Mishin, Y., 2003. Interatomic potentials for atomistic simulations of the Ti-Al system. Phys. Rev. B 68 (2), 024102.